Reports in Mechanical Engineering
Vol. 4, No. 1, 2023, pp. 104-120
ISSN: 2683-5894, DOI: https://doi.org/10.31181/rme040129072023lg

Insights about aliasing and spectral leakage when analyzing discrete-time finite viscoelastic functions

Enrique A. López-Guerra[2], Berkin Uluutku[2,3], Santiago D. Solares[1,2]

[1]Catholic University of America, USA
[2]Department of Mechanical and Aerospace Engineering, The George Washington University, USA
[3]X-wave Innovations Inc., USA

Article Info

Article history:

Received June 20, 2023
Revised July 19, 2023
Accepted July 29, 2023

Keywords:

Viscoelasticity,
Discrete-finite signals,
Discrete-Time Fourier,
Transform (DTFT),
Generalized Maxwell model,
Stress relaxation,
Aliasing,
Spectral leakage,
Frequency spectrum analysis.

ABSTRACT

Material property viscoelastic inversion studies often rely on the continuous -time framework for Fourier analysis, which may not accurately represent real experimentally collected data. In this paper, we address the discrete and finite nature of viscoelastic functions obtained from experiments and discuss the impact of these characteristics on the frequency spectrum analysis. We derive equations for the Discrete-Time Fourier Transform (DTFT) of a discrete-finite stress relaxation signal corresponding to the relaxation of a generalized Maxwell model. Our analysis highlights the limitations of the traditional continuous -time framework in capturing the inherent features of real signals, which are discrete and finite in nature. This results in two phenomena: aliasing and spectral leakage. We present equations that consider these phenomena, allowing experimentalists to anticipate and account for aliasing and leakage when performing model fitting. The proposed discrete-finite approach provides a more accurate representation of real viscoelastic data, enabling researchers to make better-informed decisions in the analysis and interpretation of sample viscoelastic functions.

Corresponding Authors:

Enrique A. López-Guerra,
The George Washington University, USA.
Email: enrique.a.lopez.guerra@gmail.com

Santiago D. Solares,
Catholic University of America, The George Washington University, USA.
Email: ssolares@gwu.edu

1. Introduction

Viscoelastic materials exhibit both viscous and elastic properties and have been the subject of extensive research due to their widespread applications in various industries, such as automotive, aerospace, and biomedical engineering (Bruner & Dauskardt, 2014; Dittmer et al., 2000; Garcia et al., 2020; López-Guerra et al., 2019; Plodinec et al., 2012). The study of viscoelastic functions is essential to understand these materials' mechanical behavior, and accurate frequency spectrum analysis plays a crucial role in characterizing their response to stress and strain (Brinson & Brinson, 2008; Ferry, 1980).

Traditionally, Fourier analysis in the field of viscoelasticity has been performed within the framework of continuous-time signals, which has been widely accepted and employed in numerous studies (Brinson & Brinson, 2008; Evans et al., 2009; Ferry, 1980; Findley et al., 1989; Geri et al., 2018; Holly et al., 1988; López-

Guerra et al., 2017; M. McCraw et al., 2021; Tassieri et al., 2012; Tschoegl, 1989; Zhai & McKenna, 2014). However, real experimental data of viscoelastic functions are inherently discrete and finite, and the use of the continuous-time framework may not accurately represent these characteristics. This discrepancy can lead to the occurrence of two phenomena: aliasing and spectral leakage, which can significantly impact the accuracy and reliability of model fitting in viscoelastic studies.

In fields such as electrical engineering and digital signal processing, the topics of aliasing and spectral leakage have been widely recognized and addressed (Lyons, 2011; McClellan et al., 2003; Oppenheim et al., 1999; Oppenheim & Schafer, 1975; Smith, 1997). Despite their importance, these concepts have not sufficiently permeated other physical science fields, including linear viscoelasticity. This lack of integration has limited the development of robust methods for analyzing the frequency spectrum of discrete-finite viscoelastic functions.

In the literature, there exist works investigating viscoelasticity in the Fourier context and discussing unexpected mismatches between the theory and experimental data due to signal properties and artifacts, such as aliasing (Aspden, 1991; Shtrauss, 2019; Shtrauss & Kalpins, 2012). In the last two years, we have made efforts to address the discrete nature of experimental data and bridge the gap between the continuous world of theory and the discrete world of experimentation. We have started our journey by exploring viscoelasticity in the Z -domain, which can be considered as a discrete counterpart to the Laplace domain commonly utilized in viscoelasticity theory derivations (Uluutku et al., 2021). We have analytically developed linear viscoelasticity models' constitutive equations in the Z-domain and compared the analytical results with experimental and simulated data. The advancements in the Z-domain have allowed us to effectively handle aperiodic and unbounded signals, which are frequently encountered in material indentation and stress-strain experiments. To streamline the newly developed methodology and establish consistency with the viscoelastic spectra and harmonic experiments, we have continued our work by focusing on certain contours of the Z -domain and carrying out the analysis on discrete modified Fourier domains (Lin et al., 2023; M. R. McCraw et al., 2022; Uluutku et al., 2022). The analytical equations derived in the Z-domain are evaluated at certain contours and reduced to variants of a single complex variable instead of a pair consisting of a real and an imaginary variable. To transition the signals into the chosen discrete modified Fourier domain, the signals are bounded via multiplication by a decaying exponential function, after which a discrete Fourier transform is executed. This method has proven to have several advantages, such as reducing the impact of spectral leakage and obtaining a modified version of the viscoelastic spectrum. This paper builds on our previous efforts and presents a unique approach by bringing the analysis back to the traditional Dicrete-Time Fourier transform (DTFT) and allowing the explicit observation of aliasing and spectral leakage within the theoretical framework.

While the theory and methodology outlined in this work are widely applicable to numerous stress conditions, we primarily focus on stress relaxation and creep analysis. This focus is motivated by the increasing interest in soft inflatable structures for space exploration and colonization missions. The accurate characterization of creep behavior in these structures is vital to ensure their sustained performance under the rigorous conditions of outer space. This study thereby underlines the necessity to devise innovative methods and techniques that can efficiently capture and evaluate the unique properties of these soft inflatable structures in challenging space environments. (The US Small Business Administration, n.d.). Our study is divided into three main parts: discussing the traditional continuous-time framework, presenting the discrete-time theoretical framework, isolating the effect of aliasing, and analyzing the impact of sequence size on spectral leakage. With analytical equations, we show that both aliasing and leakage "pollute" all frequency bins, and by using the derived DTFT equations, experimentalists can anticipate these phenomena and consider them when performing model fitting. Finally, we offer concluding remarks and suggestions for future research. In addition, an Appendix is offered with a detailed step-by-step derivation of the main equations discussed in the main manuscript.

2. Continuous-time theoretical framework

Stress relaxation defines the stress behavior of a viscoelastic material under sustained strain. In contrast, creep characterizes the strain response when the material is exposed to steady stress. Stress relaxation, creep, and harmonic (sinusoidal) loading are frequently analyzed viscoelastic responses and are generally recognized as standard viscoelastic material functions (Brinson & Brinson, 2008; Ferry, 1980; Tschoegl, 1989). Furthermore, it is established that if one standard function can be accurately measured, it is theoretically possible to infer the other two through the correct application of viscoelastic interconversions (Park & Schapery, 1999; Schapery & Park, 1999; Tschoegl, 1989). Importantly, certain interconversions are based on the Fourier transform, thereby making it a central point of focus in this study. For example, starting from stress relaxation, if we can model our material as a generalized Maxwell model with K elements, our experimental

stress relaxation data should conform to the following equation (Brinson & Brinson, 2008; Findley et al., 1989; Forstenhäusler et al., 2021; Tschoegl, 1989):

$$G(t) = \left(\{G_e\} + \sum_{k=1}^{K} G_k e^{-\frac{t}{\tau_k}} \right) u(t) \tag{1}$$

where $k = 1,2,\ldots,K$, τ_k is the k[th] relaxation time, K is the total number of relaxation times. G_k is the relaxation modulus associated with the k-th relaxation time. $G(t)$ is the relaxation modulus, and the term within curly brackets, G_e, signifies the equilibrium modulus (also called rubbery modulus), which is predominantly responsible for the mechanical response at long timescales. Representing a purely elastic response, the rubbery modulus is commonly assumed to be zero for various materials. $u(t)$ is the unit step (Heaviside) function, emphasizing that the relaxation function is zero for negative times.

The Fourier Transform, a fundamental tool in viscoelastic material interconversion, aids in extracting standard harmonic responses from gathered stress relaxation or creep data. The analysis of stress relaxation behavior can be efficiently conducted in the frequency domain, affording intuitive insights into its properties across various timescales and frequencies. Further, the frequency domain approach allows us to glean generalized information about the material's behavior from its relaxation characteristics. In this context, we highlight the Continuous-Time Fourier Transform (CTFT) to differentiate this theoretical formalism from the experimental discrete-time Fourier methods, set to be explored in ensuing sections. Thus, to represent stress relaxation in the frequency domain, we take the Fourier transform of the relaxation modulus, specifically employing the CTFT, which is defined as follows (Kreyszig, 1999; Smith, 1997):

$$\mathcal{F}\{f(t)\}(\omega) = \int_{-\infty}^{\infty} f(t) e^{-i\omega t} dt \tag{2}$$

The CTFT allows us to connect time-domain viscoelastic responses (e.g., stress relaxation, creep) with standard frequency-domain viscoelastic functions (e.g., complex modulus, complex compliance). Applying the CTFT (Equation (2)) to the stress relaxation expression for the Maxwell model (Equation (1)), we obtain the following Equation that connects the CTFT of the relaxation modulus with the Maxwell model parameters:

$$\mathcal{F}\{G(t)\} = \{G_e\}\left(\frac{1}{i\omega} + \pi\delta(\omega)\right) + \sum_{k=1}^{K} \frac{G_k \tau_k}{1 + i\omega\tau_k} \tag{3}$$

The first term corresponds to the Fourier transform of the unit step function. This is not classically defined due to the function's non-absolute integrability. However, it can be symbolically represented by a $1/i\omega$ term for the continuous spectrum and a Dirac delta function $\delta(\omega)$ term for the discontinuity at zero frequency, indicating the unit step function's abrupt change at the origin (Oppenheim et al., 1999).

If we multiply Equation (3) by $i\omega$ we obtain:

$$(i\omega) \cdot \mathcal{F}\{G(t)\} = \{G_e\}\big(1 + i\omega\pi\delta(\omega)\big) + \sum_{k=1}^{K} \frac{G_k \tau_k i\omega}{1 + i\omega\tau_k} \tag{4}$$

When the Fourier transform is multiplied by $i\omega$, the term $i\omega\pi\delta(\omega)$ arises. However, due to the unique nature of the delta function, which is only defined at $\omega = 0$, the term $i\omega\pi\delta(\omega)$ essentially disappears at $\omega = 0$, since the omega factor serves as a zero multiplier. This term, while theoretically present, does not materially affect practical engineering applications and thus can be rightfully set aside:

$$(i\omega) \cdot \mathcal{F}\{G(t)\} = \{G_e\} + \sum_{k=1}^{K} \frac{G_k \tau_k i\omega}{1 + i\omega\tau_k} \tag{5}$$

From this last equation, it is recognized that the right-hand-side is the complex modulus, $G^*(\omega)$, of a Generalized Maxwell model with an arbitrary number of K elements [6, 8]. The complex modulus, $G^*(\omega)$, represents the harmonic stress response in the steady state for a material subjected to harmonic strain excitation.

Thus, Equation (5) can also be expressed as:

$$(i\omega) \cdot \mathcal{F}\{G(t)\} = G^*(\omega) \tag{6}$$

This is a well-known expression connecting the CTFT of the relaxation modulus ($\mathcal{F}\{G(t)\}$) with the complex modulus ($G^*(\omega)$) (Findley et al., 1989; Tschoegl, 1989). The complex modulus ($G^*(\omega)$) offers a convenient pathway to ascertain the complex compliance, defined as its inverse:

$$J^*(\omega) = 1/G^*(\omega) \tag{7}$$

This complex compliance embodies the frequency-domain analog of the creep behavior—a material's time-dependent strain under sustained stress. Thus, while creep measures how a material strain evolves with time under a constant stress in the time-domain, the complex compliance describes the material's response under a sinusoidal (or harmonic) stress variation in the frequency domain. Therefore, $J^*(\omega)$ serves as an insightful metric to characterize a material's frequency-dependent viscoelastic behavior during creep.

3. Discrete-time theoretical framework

The significance of discrete-time data in viscoelasticity studies is paramount, largely due to the inherent nature of data collection through modern digital instrumentation, which naturally produces discrete series of data (Uluutku, 2022). In viscoelastic characterization, constant deformation or load application is a common practice for stress relaxation and creep assessment, respectively. In an experimental setting that involves the application of constant strain deformation, our discrete-time relaxation data (represented as $x[n]$) assumes the form:

$$x[n] = u[n] \cdot \left(\sum_{k=1}^{K} G_k e^{-t[n]/\tau_k} + \{G_e\} \right), \quad n = 1,2,\dots,\infty \tag{8}$$

where, as before, $k = 1,2,\dots,K$, τ_k is the k[th] relaxation time, K is the total number of relaxation times, G_e is rubbery modulus, G_k is the relaxation modulus associated with the k-th relaxation time, Δt is the experimental timestep whose inverse is known as the sampling frequency, and $u[n]$ is the (Heaviside) unit step function. Having a unit step function in the expression indicates that before the experiment, before time zero, the material is in resting conditions with no priori deformation or stress. Equation (8) serves as the discrete-time equivalent of Equation (1), marking our transition from continuous to discrete notation. It is important to underline that $x[n]$, the discrete relaxation data, is a sequence that relies on the index '*n*,' rather than on a continuous -time variable. Observations occur at distinct time points, represented as the discrete series $t[n]$. In cases where the sampling time is constant, we can replace the series containing time with $t[n] = n\Delta t$, where Δt is the constant sampling time. This simplifies the notation without loss of information. Hence the relaxation behavior can be described by:

$$x[n] = u[n] \cdot \left(\sum_{k=1}^{K} G_k e^{-n\Delta t/\tau_k} + \{G_e\} \right), \quad n = 1,2,\dots,\infty \tag{9}$$

Making the substitution: $a_k = e^{-\Delta t/\tau_k}$, the summation term would become: $\sum_{k=1}^{K} G_k a_k^n$. This substitution may become handy for further simplifications (see Appendix).

Although these viscoelastic functions are generally regarded as bandwidth unlimited, it is illustrative to notice that their low-frequency and large-frequency responses are dominated by the inverse of the largest ($1/\tau_K$) and lowest relaxation time ($1/\tau_1$), respectively. Illustration of Equation (9) with different sampling frequencies, $1/\Delta t$, can be seen in Figure 1.

In the continuous-time framework covered in the previous section, we used the CTFT on the time-domain relaxation modulus (Equation (2) applied to Equation (1)), yielding a frequency-domain relationship related to the complex modulus. In contrast, in the discrete-time scenario, we apply its analog, the DTFT, to our sequence. The DTFT employs a discrete infinite summation on the sequence elements, resulting in a transformed function in the continuous frequency variable Ω:

$$X(e^{i\Omega}) = \sum_{n=-\infty}^{\infty} x[n] e^{-j\Omega n} \tag{10}$$

where the frequency Ω ranges from zero to 2π. This unit circle agle unit, Ω, corresponds to a range from $-\left(\frac{1}{2\Delta t}\right)$ to $\left(\frac{1}{2\Delta t}\right)$. Although the signal is discrete in time, we obtain a continuous expression in frequency as a result of the DTFT. When we have a time-limited signal, we cannot apply the DTFT, except for a handful of scenarios where the data is well-windowed and bounded between trailing zero values. For time-limited series, we can only apply the discrete Fourier transform (DFT), which inherently assumes the sequence to be periodic. This may also introduce some artifacts for unbounded signals; however, it is very practical and utilized in every aspect of engineering and applied sciences. The analytical equations derived for the DTFT also hold for the DFT. One can visualize the DFT as a sampled version of the DTFT where we pick equally spaced data points in the amount of sequence length on Ω. Therefore, in contrast to the DTFT, the resulting frequency signal is also discrete, just like the time signal. It is very easy to confuse the DFT, DTFT, and other Fourier family transformations due to their similar names, and more information can be found in references (Smith, 1997; Uluutku et al., 2021). Although one can calculate the DFT by other means and from formal definitions, it is

much more convenient and efficient to utilize well-established algorithms such as the Fast Fourier Transform (FFT) (Cooley & Tukey, 1965).

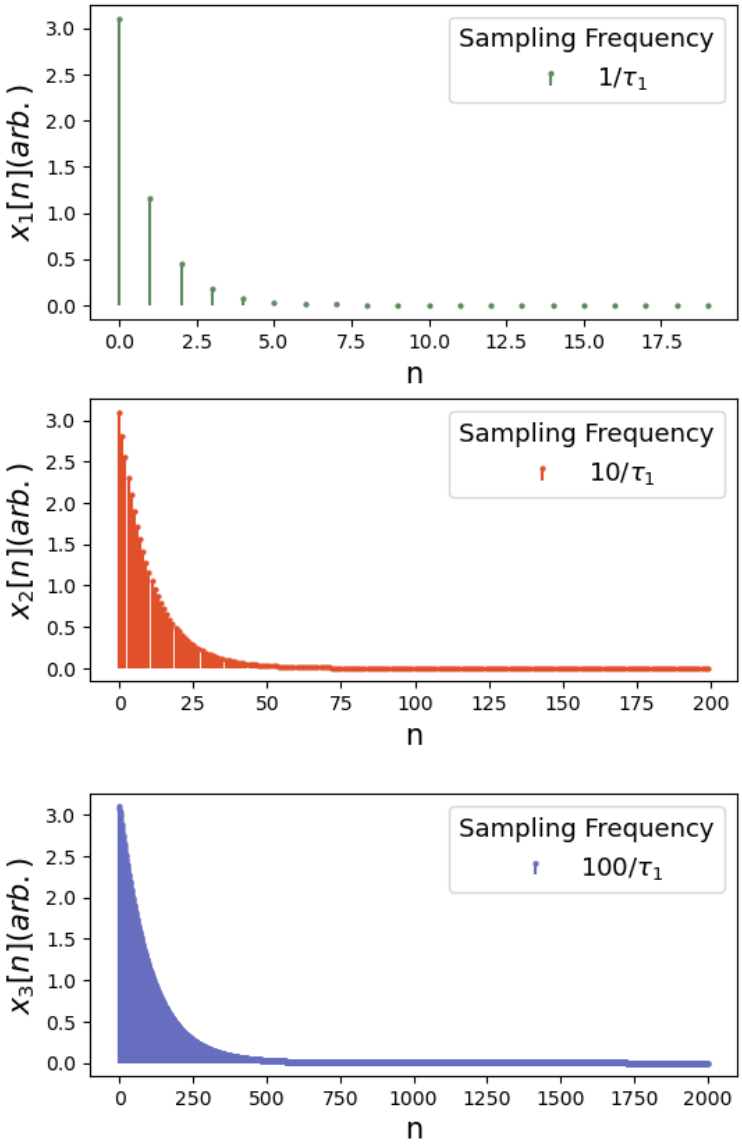

Figure 1. Graphical representations of the discrete-time relaxation modulus described in Equation (9) for three different sampling frequencies shown in the figure legends. Note that the x-scales are different but covering the same region of the exponential decay. The upper plot shows very few non-zero samples available when the sampling frequency is chosen as $(1/\tau_1)$ whereas, in the extreme case, the lower plot shows a sampling frequency of $100/\tau_1$. The middle plot is a middle ground with a sampling frequency of $10/\tau_1$. In the following section, we will delve into the impact of choosing different sampling frequencies on the frequency analysis of signals.

Applying the DTFT operation to the discrete relaxation modulus defined in Equation (9), we can obtain the relaxation modulus in the frequency domain as follows (A detailed derivation can be found in the Appendix):

$$X(e^{i\Omega}) = \Delta t \frac{\{G_e\}}{1 - e^{-i\Omega}} + \Delta t\{G_e\} \sum_{r=-\infty}^{\infty} \pi\delta(\Omega - 2\pi r) + \Delta t \sum_{k=1}^{K} \frac{G_k}{1 - e^{-\Delta t/\tau_k} e^{-i\Omega}} \tag{11}$$

As Δt approaches zero, we approach a continuous signal, and the Equation starts to converge to the continuous formalism. For small values of the sampling time, Δt, (in other words, for high sampling frequencies), we can simplify Equation (11) utilizing a Taylor expansion. By doing so and neglecting higher order terms in Δt as for the cases where it is small (see Appendix for details on the simplification), we obtain:

$$X(i\omega) \sim \{G_e\}\left(\frac{1}{i\omega} + \Delta t \sum_{r=-\infty}^{\infty} \pi\delta(\Omega - 2\pi r)\right) + \sum_{k=1}^{K} \frac{G_k \tau_k}{1 + i\omega\tau_k - i\omega\Delta t} \quad (12)$$

Now when we compare the frequency-domain equations between the continuous-time case (Equation (3)) and the discrete-time case (Equation (12)), we observe that they have the same shape but differ by an additional term $(-i\omega\Delta t)$ in the denominator. It is insightful to note that this term diverges the discrete formulation from the continuous formulation. Therefore, not considering this term and using a continuous formulation with discrete data causes inaccuracies.

3. Effects of Upper-bandwidth limit (Aliasing)

The DTFT frequency axis spans from minus to plus the Nyquist rate, which is one over half the sampling period or the half sampling frequency. The selection of an appropriate sampling frequency directly affects the accurate representation of the signal and underlying physics. Selection of the upper bandwidth limit is essential as one would like to sample at a rate that is at least twice the highest frequency present in a signal to satisfy Nyquist-Shannon sampling theorem and to be able to reconstruct the continuous signal from the sampled one. If this criterion is not satisfied, the signal cannot be represented accurately. Now, clearly The relaxation equation contains every frequency (Equation (3)). Therefore, it is technically impossible to select a sampling frequency at least twice the higher frequency. However, the frequency components do become negligible beyond a certain point, and we can always choose a "practical highest frequency." To demonstrate this, we choose three different sampling frequencies that are scaled to the relaxation time, $1/\tau_1$. The selection of these three sampling rates is illustrated in Figure 2. To visualize the meaning of this illustration, one can consider that each sampling frequency in the plotted spectrum only allows accurate representation of the portion of the signal up to its respective vertical line. The portion of the signal that is not contained to the left of the respective line will be "folded back," aliased, and will pollute the spectrum. For example, we can expect serious aliasing and inaccuracies with $1/\tau_1$ sampling frequency. Meanwhile, little and minimal aliasing would be observed with $10/\tau_1$ and $100/\tau_1$, respectively. Therefore, the sampling rate must be at least twice higher than the bandwidth of the signal; this determines the upper bandwidth limit.

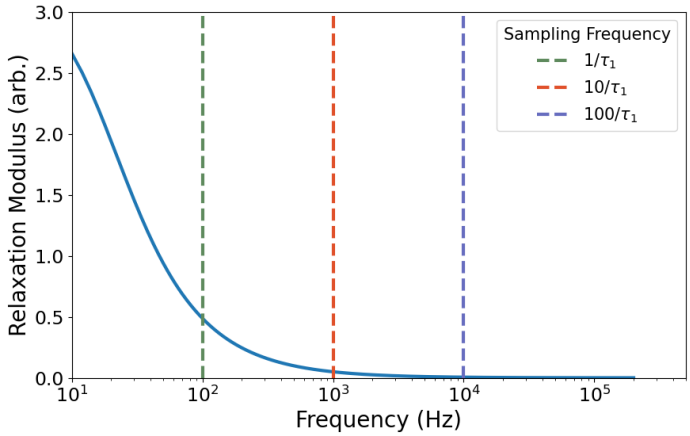

Figure 2. Continuous-time Fourier Transformed representation of the relaxation modulus for three choices of upper bandwidth limit, given by the three vertical dashed lines: a) $1/\tau_1$, b) $10/\tau_1$, c) $100/\tau_1$. For $100/\tau_1$ it can be seen that the frequency components (magnitude of the signal) are negligible. The effects of the sampling frequency in the time domain are illustrated in Figure 1 and the effects on the transformed data in the frequency domain are illustrated in Figure 3.

In the discrete formulation of the generalized Maxwell model, Equation (12), where we need to include a sampling frequency, we can see this aliasing effect prominently. Changing the sampling rate, especially making it significantly smaller, disturbs the data and makes the resulting transform diverge from the continuous case significantly. This phenomenon, known as aliasing, is encapsulated in the $(-i\omega\Delta t)$ term of Equation (12) and its effect is illustrated in Figure 3. When computing the DFT of stress relaxations for different sampling rates, as illustrated in Figure 3, the signal with a $1/\tau_1$ sampling rate noticeably deviates from the continuous formulation (Equation (3)). Consequently, data affected in this manner must be processed within the context

of a discrete-time framework. Upon closer observation, it is apparent that the DFT of the data harmonizes precisely with the stress relaxation calculated analytically using the discrete formulation (Equation (12)).

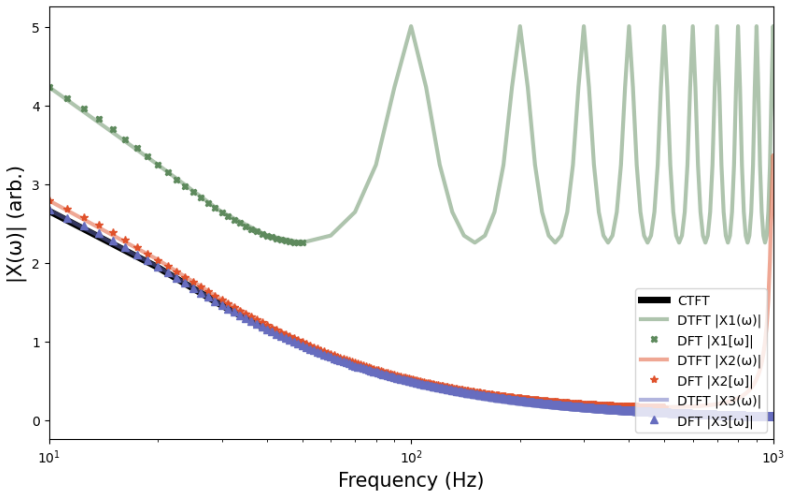

Figure 3. Comparative DTFT analysis for the three different selections of sampling frequency shown in Figure 1 and Figure 2. The green trace represents $|X_1(\omega)|$, and underscores an extreme case of significant frequency aliasing due to a sampling frequency of $1/\tau_1$ Hz, causing a notable departure from the continuous-time CTFT, represented by the black continuous line. $|X_2(\omega)|$ and $|X_3(\omega)|$ have higher sampling frequencies ($10/\tau_1$ and $100/\tau_1$ Hz, respectively) and therefore follow more closely the theoretical CTFT line, as frequency aliasing is less prominent in these two cases. Regardless of whether aliasing is expected, data subject to such effects must be analyzed within a discrete-time framework. On careful examination, the DFT of the data aligns precisely with the analytically computed stress relaxation using the discrete formulation (Equation (12)). Recall that the DFT, a sampled version of the DTFT, can be practically implemented through various software packages, and in this case, was computed using the popular FFT algorithm (Cooley & Tukey, 1965) via the Python scipy package (Virtanen et al., 2020).

4. Effects of Signal Length (Spectral Leakage)

So far, we have examined the implications of using a discrete-time signal instead of a continuous function, as well as the consequences of the selected sampling frequencies and related aliasing effects. Until now, we have also assumed the signals to be infinitely long for the purpose of discussion. However, actual experimental data consists of finite sets. In this section, we shift our focus to the effects of signal length and, consequently, the duration of the experiment. Now we consider a similar relaxation modulus sequence like that of Equation (9), but this time we will assume that the sequence is finite with an "M" number of elements.

$$y[n] = (u[n]) \cdot \left(\sum_{k=1}^{K} G_k e^{-n\Delta t/\tau_k} + \{G_e\} \right), \quad n = 1,2,\dots,M \tag{13}$$

After the time point M, we do not have any information about the behavior of the signal; however, if we multiply this function with a rectangular pulse with the width of M that would span the known part of the signal, we can window the known parts of the signal. The unknown parts of the signal would be multiplied by zero; hence we can write the new expression as:

$$y[n] = (u[n] - u[M]) \cdot \left(\sum_{k=1}^{K} G_k e^{-n\Delta t/\tau_k} + \{G_e\} \right), \quad n = 1,2,\dots,\infty \tag{14}$$

The above equation is illustrated in Figure 4 with three different signal lengths.

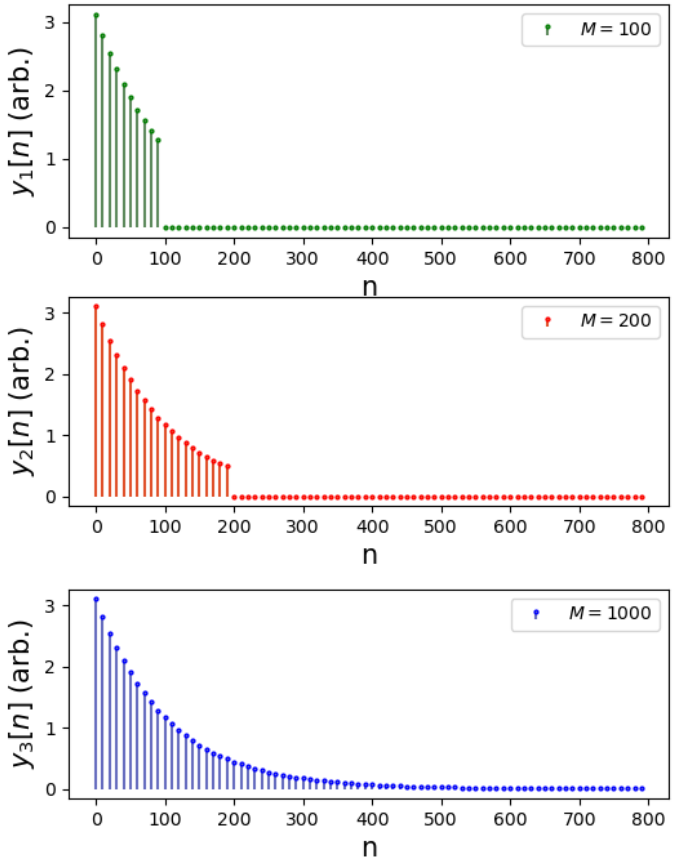

Figure 4. Time-domain representation of discrete-time stress relaxation data with three different experimental lengths conforming to Equation (14). The aim is to explore the influence of these sequences' lengths on their Fourier spectra when the DTFT is applied. A detailed examination of the consequences of this truncation can be found in Figure 5.

Since by windowing, we have obtained an infinite length function; we can apply the DTFT and find the stress relaxation in the frequency domain. Although we are still using the generalized Maxwell model, the presence of the rectangular window function alters the Fourier response. First, the windowing operation of the unknown parts of the signal corresponds to zero padding. As mentioned above, when DFT is applied to a finite signal, the resulting signal in the frequency domain is also finite. However, by zero-padding the signal to infinity, we are making the frequency continuous. Essentially, by zero padding, we are interpolating the frequency response artificially, which does not alter the frequency data points of the DFT. However, it causes interpolated parts of the signal to have artificial oscillations. Second, not having the full signal, to begin with, causes a loss of information and causes spectral leakage. The DTFT of the windowed signal is expressed as follows. A detailed derivation can be found in the Appendix.

$$Y(e^{j\Omega}) = \Delta t\left\{\frac{G_e(1-e^{-iM\Omega})}{1-e^{-i\Omega}}\right\} + \Delta t\sum_{k=1}^{K}\frac{G_k(1-e^{-M\Delta t/\tau_k}e^{-iM\Omega})}{1-e^{-\Delta t/\tau_k}e^{-i\Omega}} \tag{15}$$

Equation (15) represents the DFT of the discrete-time, finite M-size stress relaxation sequence for a generalized Maxwell model, encompassing an arbitrary K number of relaxation times as given in Equation (7). This equation incorporates the contribution of the rubbery modulus Ge, making it a more comprehensive theoretical framework. Now, we perform Taylor series expansions as in previous section and higher order terms in Δt as for the cases where it is small (see Appendix for details on the simplification) we obtain:

$$Y(i\omega) \sim \left\{\frac{G_e(1-e^{-i\omega\Delta tM})}{i\omega}\right\} + \sum_{k=1}^{K}\frac{G_k\tau_k(1-e^{-M\Delta t/\tau_k}e^{-iM\omega\Delta t})}{1+i\omega\tau_k-i\omega\Delta t} \tag{16}$$

Note that in the numerator, we cannot neglect higher order terms on $M\Delta t$ in the Taylor series expansion. Whereas Δt tends to be small for higher sampling frequencies, M also may tend to be large as more data points

of the experimental relaxation sequence are available. It is evident that as M increases, the term $e^{-M\Delta t/\tau_k}e^{-iM\omega\Delta t}$ diminishes, thereby mitigating the effect of spectral leakage.

The impacts of aliasing and spectral leakage, resulting from the finite and discrete nature of the data sequences, are encapsulated in Equation (16). As Figure 5 graphically illustrates, these impacts are sensitive to sequence size, influencing the Fourier spectrum. For shorter signals, an oscillatory behavior emerges due to spectrum interpolation via zero-padding. This not only 'fills the frequency gaps,' but also significantly alters the overall magnitude and distribution of the signal.

As the known section of the sequence expands and the data becomes more and more bounded, the Discrete Time Fourier Transform (DTFT) gradually converges to the Continuous -Time Fourier Transform (CTFT). This occurs when the exponentially decaying terms in the relaxation function have substantially decayed before data capture is halted. This suggests that choosing a sufficiently large M value can effectively mitigate the spectral leakage effect.

However, in practice, constraints such as experiment duration and data storage often preclude the acquisition of long sequences. This reality underscores the value of the mathematical framework proposed in Equation (15), which takes into account the effects of aliasing and leakage. By doing so, this framework provides a more accurate and pragmatic theoretical tool for analyzing real-world, finite, discrete-time viscoelastic signals.

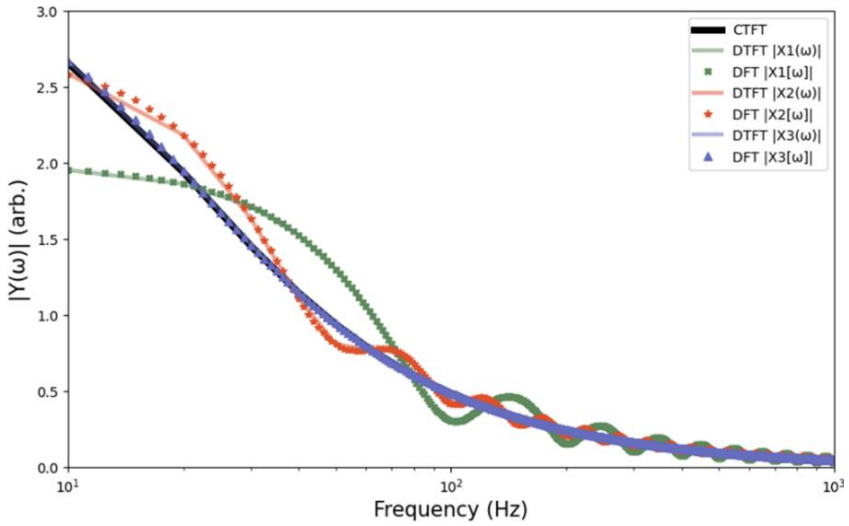

Figure 5. Effect of the length of the sequence, M, (spectral leakage effect) on the Fourier spectra of the three sequences with different M shown in Figure 4. The value of M is 100, 200, and 1000 for $Y_1(\omega), Y_2(\omega), Y_3(\omega)$, respectively. The continuous (yellow) line shows the theoretical Fourier spectrum of the relaxation modulus for the continuous-time function. It can be clearly seen that the shorter the sequence, the higher the "ripple" effect and the further the trace deviates from the theoretical value. This "ripple" effect is clearly originating from the term $e^{-M\Delta t/\tau_k}e^{-iM\omega\Delta t}$ in Equation (12). It can be easily seen that as M goes to infinity, the real part (amplitude) of this term goes to zero and the effect of spectral leakage vanishes. This underlines the fact that data subject to such effects must be analyzed within a discrete-time framework that accounts for finite-sequences. In other words, if we have finite and discrete stress relaxation data as that collected in a real -life experiment, we should use Equations (15) and (16) instead of the classical time-continuous formulations (Equation (3)).

As a summarizing note, Figure 6 provides a comparative overview of Fourier analysis applied to viscoelastic stress relaxation signals under different scenarios: an infinitely long discrete-time sequence, a discrete and finite sequence (as observed in real-life cases), and the continuous-time case for reference. For ease of understanding, we have highlighted the terms that deviate from the traditional continuous-time theoretical formulation.

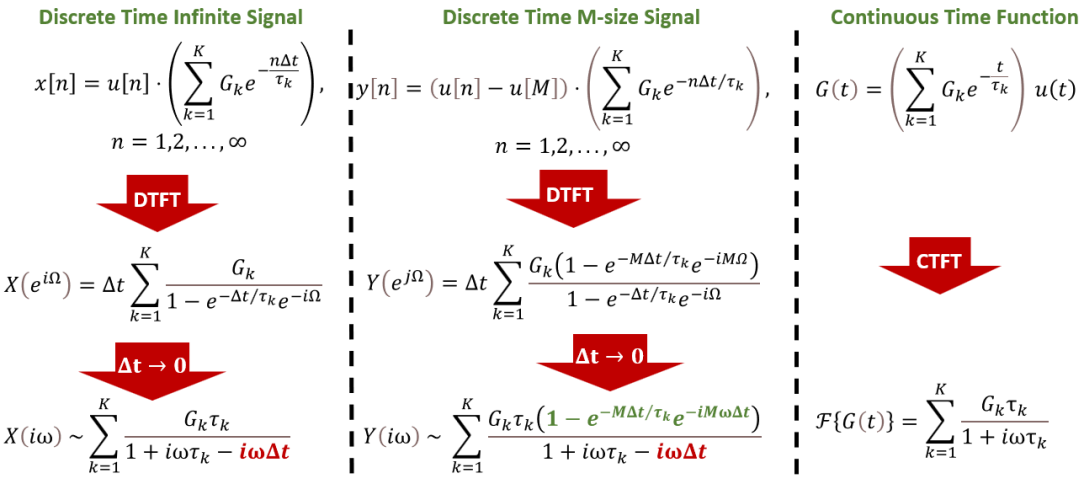

Figure 6. Comparison of mathematical formulations in Fourier analysis applied to viscoelastic stress relaxation signals for the following three specific cases: an infinite discrete-time sequence (left-hand-side), a finite discrete sequence indicative of real-world scenarios (center), and the continuous-time classical formulation (right-hand-side). After applying certain approximations (refer to Appendix A), the discrete-time cases (Equation (12)) demonstrate similarity to the continuous-time case (Equation (3) on right-hand-side). However, the discrete-time cases have an additional term ($i\omega\Delta t$) in the denominator, which is associated with the aliasing effect. Further, the finite discrete-time case (Equation (16) in the central image) introduces another term in the numerator ($1 - e^{-M\Delta t/\tau_k} e^{-iM\omega\Delta t}$), considered to be the origin of spectral leakage due to the truncation of the M-sized length sequence. While our derived equations in the main text encompass the rubbery modulus term, this figure deliberately omits it for the sake of clarity, allowing for a more focused comparison with the continuous-time case. Nonetheless, the inclusion of the rubbery modulus term may be pertinent in some cases based on the specifics of the analysis.

5. Practical Illustration of the Discrete-Finite Approach in Extracting Viscoelastic Properties

We now turn our attention to Figure 7, which underscores the importance of our discrete and finite approach to experimental time-domain stress relaxation data analysis. Figure 7A illustrates a simulated time-domain stress relaxation signal. This simulation employs generalized Maxwell parameter data for polyisobutylene from Brinson, Catsiff, and Tobolsky (Brinson & Brinson, 2008; Catsiff & Tobolsky, 1955), a sampling frequency of 44.45 MHz, a total sampling time of 92 μs, and incorporates Gaussian noise. The code utilized for this simulation and data analysis is fully accessible in (Lopez-Guerra, 2023/2023). This form of discrete and finite digital data, featuring noise, mirrors the typical output obtained from modern high-frequency digital equipment used in actual rheological experiments.

In Figure 7B, the Fourier transform analysis of the time-domain data from Figure 7A is displayed. Here, we show four traces: the Discrete-Time Fourier Transform (DTFT) calculated with Equation (15), the numerical Fast Fourier Transform (FFT) represented by blue asterisks, the Continuous-Time Fourier Transform (CTFT) based on the conventional continuous-time case (Equation (3)), and a nonlinear least square fit using Equation (15) as the fitting model. By also applying nonlinear least square (NLLS) fitting with Equation (3) as the fitting model, we emphasize the risks associated with traditional theoretical formalisms. Both nonlinear optimizations were performed using the open source lmfit python package (Newville et al., 2016).

Figure 7C offers a comparison of actual (theoretical) material properties and those estimated when using different theoretical frameworks. The theoretical complex modulus, calculated with Brinson, Catsiff, and Tobolsky's Maxwell parameter data for poly isobutylene (Brinson & Brinson, 2008; Catsiff & Tobolsky, 1955), is contrasted with the complex modulus extracted through our discrete-finite framework (Equation (15)) and the continuous-time framework (Equation (3)). The comparisons presented clearly underscore the improved accuracy offered by our discrete and finite theoretical approach, underscoring its necessity for the precise interpretation of viscoelastic data. It is important to point out that the Fourier analysis is tailored to the specific region of interest, which corresponds to the experimental timescale. That is, the frequency region spans from $1/T$ to $1/\nu_f$, where T and ν_f denote the total experimental time and the sampling frequency, respectively. Note that in Figure 7C, the complex modulus for all traces is calculated using Equation (5). For the theoretical case (orange trace), we use Maxwell parameters from Brinson, Catsiff, and Tobolsky, as previously mentioned (Brinson & Brinson, 2008; Catsiff & Tobolsky, 1955). For the discrete-finite case (blue trace) and the

continuous-time framework (green trace), we apply the parameters fitted from the NLLS optimization using Equation (15) and Equation (3), respectively.

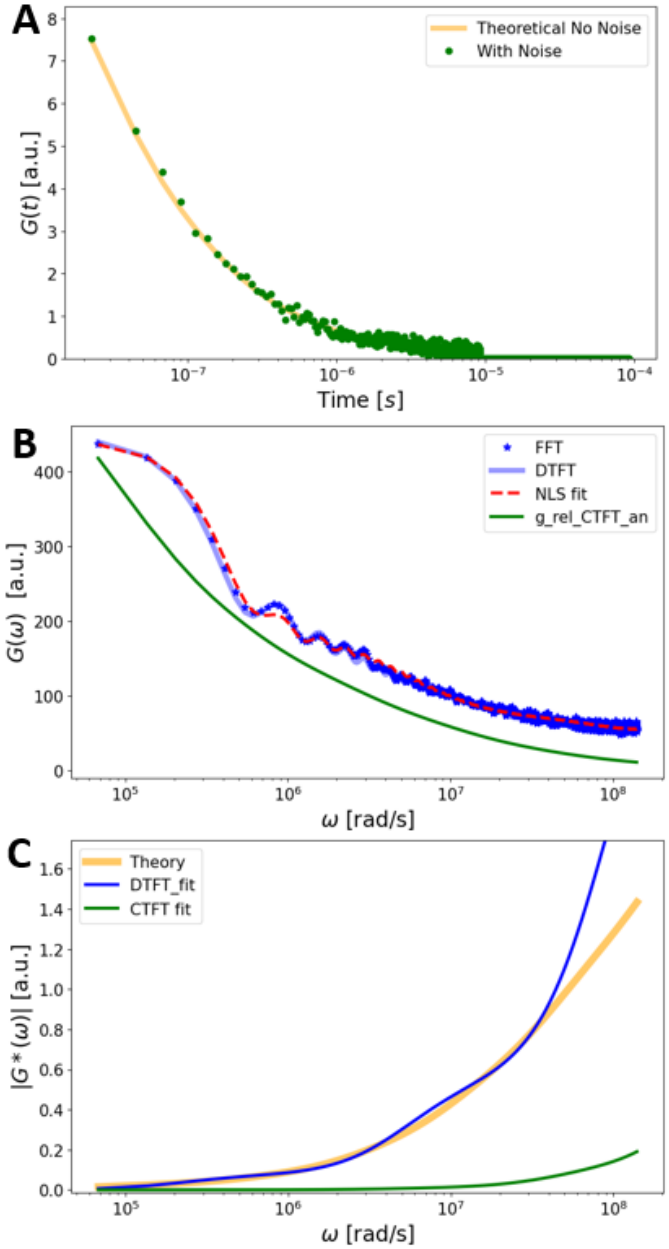

Figure 7. Importance of considering the discrete and finite nature of experimental time-domain stress relaxation data. Figure 7A shows a simulated time-domain stress relaxation signal generated from Maxwell parameter data for polyisobutylene (Brinson & Brinson, 2008; Catsiff & Tobolsky, 1955) with a 44.45 MHz sampling frequency over 92 μs and Gaussian noise inclusion. The simulation code is detailed in (Lopez-Guerra, 2023/2023). Figure 7B depicts the Fourier analysis of Figure 7A data, highlighting four traces: the DTFT (Equation (15), thick blue line); the numerical FFT (blue asterisks); the CTFT (continuous case formalism, Equation (3), continuous green line); and a nonlinear least square fit (red dashed line), demonstrating the risks of using the conventional continuous-time theory. Figure 7C contrasts the theoretical complex modulus (using Maxwell parameters for polyisobutylene, (Brinson & Brinson, 2008; Catsiff & Tobolsky, 1955)) with those estimated using Equation (15) versus Equation (3). The differences underscore the superior accuracy of the discrete-finite approach (Equation (15), blue continuous line) over the continuous-time formalism (Equation (3)).

As shown, the complex modulus derived from the Nonlinear Least Squares (NLLS) fitting, with Equation (15) as the objective model, closely mirrors the theoretical complex modulus over most of the frequency range. The fitting is somewhat less precise in the upper range, likely due to the relatively fewer data points at shorter timescales when analyzed on a logarithmic scale. Despite this, the discrete-finite approach is markedly more reliable than the conventional continuous-time analysis (Equation (3)), which fails to accurately track the theoretical complex modulus throughout the entirety of the analysis range.

5. Conclusion

In this study, we have demonstrated the significance of considering the discrete and finite nature of real experimentally collected viscoelastic functions when analyzing their frequency spectrum. By deriving equations for the DTFT of a discrete-finite stress relaxation signal following the relaxation of a generalized Maxwell model, we have highlighted the limitations of the traditional continuous-time framework. Our approach successfully addressed the phenomena of aliasing and spectral leakage, which were found to be crucial factors affecting the accuracy and reliability of model fitting in previous viscoelasticity studies.

The discrete-finite approach presented in this paper offers a more accurate representation of real viscoelastic data, allowing researchers to better understand and interpret viscoelastic functions. Our findings can contribute to the development of more robust methods for studying viscoelastic materials and provide guidance for experimentalists in optimizing their data analysis techniques. As a future direction, we envision extending the application of our approach to additional viscoelastic models and exploring its relevance within other types of viscoelastic responses such as those observed during the application of a linear time-dependent force, a topic of significant interest in modern characterization techniques like force-distance curve spectroscopy in atomic force microscopy, among others.

References

Dittmer, J. J.; Lazzaroni, R.; Leclère, P.; Moretti, P.; Granström, M.; Petritsch, K.; Marseglia, E. A.; Friend, R. H.; Brédas, J. L.; Rost, H.; Holmes, A. B. *Sol. Energy Mater. Sol. Cells* 2000, *61*, 53–61. doi:10.1016/S0927-0248(99)00096-3

Plodinec, M.; Loparic, M.; Monnier, C. A.; Obermann, E. C.; Zanetti-Dallenbach, R.; Oertle, P.; Hyotyla, J. T.; Aebi, U.; Bentires-Alj, M.; Lim, R. Y. H.; Schoenenberger, C.-A. *Nat. Nanotechnol.* 2012, *7*, 757–765. doi:10.1038/nnano.2012.167

Bruner, C.; Dauskardt, R. *Macromolecules* 2014, *47*, 1117–1121. doi:10.1021/ma402215j

López-Guerra, E. A.; Shen, H.; Solares, S. D.; Shuai, D. *Nanoscale* 2019, *11*, 8918–8929. doi:10.1039/C8NR10287B

Garcia, P. D.; Guerrero, C. R.; Garcia, R. *Nanoscale* 2020, *12*, 9133–9143. doi:10.1039/C9NR10316C

Brinson, H. F.; Brinson, L. C. *Polymer Engineering Science and Viscoelasticity*; Springer US: Boston, MA, 2008. doi:10.1007/978-0-387-73861-1

Ferry, J. D. *Viscoelastic Properties of Polymers*, 3d ed.; Wiley: New York, 1980

Tschoegl, N. W. *The Phenomenological Theory of Linear Viscoelastic Behavior: An Introduction*; Springer-Verlag: Berlin ; New York, 1989

Findley, W. N.; Lai, J. S.; Onaran, K. *Creep and Relaxation of Nonlinear Viscoelastic Materials: With an Introduction to Linear Viscoelasticity*; Dover books on engineering; Dover: New York, 1989

López-Guerra, E. A.; Eslami, B.; Solares, S. D. *J. Polym. Sci. Part B Polym. Phys.* 2017, *55*, 804–813. doi:10.1002/polb.24327

Zhai, M.; McKenna, G. B. *J. Polym. Sci. Part B Polym. Phys.* 2014, *52*, 633–639. doi:10.1002/polb.23470

McCraw, M.; Uluutku, B.; Solares, S. *Rep. Mech. Eng.* 2021, *2*, 156–179. doi:10.31181/rme200102156m

Geri, M.; Keshavarz, B.; Divoux, T.; Clasen, C.; Curtis, D. J.; McKinley, G. H. *Phys. Rev. X* 2018, *8*, 041042. doi:10.1103/PhysRevX.8.041042

Evans, R. M. L.; Tassieri, M.; Auhl, D.; Waigh, T. A. *Phys. Rev. E* 2009, *80*, 012501. doi:10.1103/PhysRevE.80.012501

Tassieri, M.; Evans, R. M. L.; Warren, R. L.; Bailey, N. J.; Cooper, J. M. *New J. Phys.* 2012, *14*, 115032.

doi:10.1088/1367-2630/14/11/115032

Holly, E. E.; Venkataraman, S. K.; Chambon, F.; Henning Winter, H. *J. Non-Newton. Fluid Mech.* 1988, *27*, 17–26. doi:10.1016/0377-0257(88)80002-8

Lyons, R. G. *Understanding Digital Signal Processing*, 3rd ed.; Prentice Hall: Upper Saddle River, NJ, 2011

Oppenheim, A. V.; Schafer, R. W.; Buck, J. R. *Discrete-Time Signal Processing*, 2nd ed.; Prentice Hall: Upper Saddle River, N.J, 1999

Oppenheim, A. V.; Schafer, R. W. *Digital Signal Processing*; Prentice-Hall: Englewood Cliffs, N.J, 1975

McClellan, J. H.; Schafer, R. W.; Yoder, M. A. *Signal Processing First*, International ed.; Pearson Education: Hemel Hempstead, 2003

Smith, S. W. *The Scientist and Engineer's Guide to Digital Signal Processing*, 1st ed.; California Technical Pub: San Diego, Calif, 1997

Aspden, R. M. *J. Phys. Appl. Phys.* 1991, *24*, 803–808. doi:10.1088/0022-3727/24/6/002

Shtrauss, V. *WSEAS Trans. Appl. Theor. Mech.* 2019, *14*, 212–221

Shtrauss, V.; Kalpins, A. *WSEAS Trans. Appl. Theor. Mech.* 2012, *7*, 29–38

Uluutku, B.; López-Guerra, E. A.; Solares, S. D. *Beilstein J. Nanotechnol.* 2021, *12*, 1063–1077. doi:10.3762/bjnano.12.79

Uluutku, B.; McCraw, M. R.; Solares, S. D. *J. Appl. Phys.* 2022, *131*, 165101. doi:10.1063/5.0088523

McCraw, M. R.; Uluutku, B.; Solomon, H. D.; Anderson, M. S.; Sarkar, K.; Solares, S. D. 2022. doi:10.48550/ARXIV.2210.00617

Lin, L.; McCraw, M. R.; Uluutku, B.; Liu, Y.; Yan, D.; Soni, V.; Horkowitz, A.; Yao, X.; Limanowski, R.; Solares, S. D.; Beilis, I. I.; Keidar, M. *Langmuir* 2023. doi:10.1021/acs.langmuir.2c03181

The US Small Business Administration. https://www.sbir.gov/node/2291769

Park, S. W.; Schapery, R. A. *Int. J. Solids Struct.* 1999, *36*, 1653–1675. doi:10.1016/S0020-7683(98)00055-9

Schapery, R. A.; Park, S. W. *Int. J. Solids Struct.* 1999, *36*, 1677–1699. doi:10.1016/S0020-7683(98)00060-2

Forstenhäusler, M.; López-Guerra, E. A.; Solares, S. D. *Facta Univ. Ser. Mech. Eng.* 2021, *19*, 133–153

Kreyszig, E. *Advanced Engineering Mathematics*, 8th ed.; Wiley: New York, 1999

Uluutku, B. Developments for Soft-Matter Characterization in Atomic Force Microscopy. PhD Thesis, The George Washington University, 2022

Cooley, J. W.; Tukey, J. W. *Math. Comput.* 1965, *19*, 297–301. doi:10.1090/S0025-5718-1965-0178586-1

Virtanen, P.; Gommers, R.; Oliphant, T. E.; Haberland, M.; Reddy, T.; Cournapeau, D.; Burovski, E.; Peterson, P.; Weckesser, W.; Bright, J.; van der Walt, S. J.; Brett, M.; Wilson, J.; Millman, K. J.; Mayorov, N.; Nelson, A. R. J.; Jones, E.; Kern, R.; Larson, E.; Carey, C. J.; Polat, İ.; Feng, Y.; Moore, E. W.; VanderPlas, J.; Laxalde, D.; Perktold, J.; Cimrman, R.; Henriksen, I.; Quintero, E. A.; Harris, C. R.; Archibald, A. M.; Ribeiro, A. H.; Pedregosa, F.; van Mulbregt, P. *Nat. Methods* 2020, *17*, 261–272. doi:10.1038/s41592-019-0686-2

Catsiff, E.; Tobolsky, A. V. *J. Colloid Sci.* 1955, *10*, 375–392. doi:10.1016/0095-8522(55)90052-0

Lopez-Guerra, E. A. Ealopez/DTFT_viscoelasticity, 2023. (https://github.com/ealopez/DTFT_viscoelasticity)

Newville, M.; Stensitzki, T.; Allen, D. B.; Rawlik, M.; Ingargiola, A.; Nelson, A. *Astrophys. Source Code Libr.* 2016, ascl:1606.014

Appendix 1: Derivation of DTFT for an infinite sequence

We start by providing a step-by-step derivation of the DTFT of Equation (8) in the main manuscript. Equation (8) is the generalized Maxwell stress relaxation sequence where we assume that we have infinite information on the long timescale.

$$x[n] = u[n] \cdot \left(\sum_{k=1}^{K} G_k a_k^n + \{G_e\} \right), \quad n = 1,2,\dots,\infty \tag{A1}$$

where $a_k = e^{-\Delta t/\tau_k}, \quad k = 1,2,\dots,K.$

Now, we proceed to perform the DTFT (Equation (10)) $X(e^{i\Omega}) = \sum_{n=-\infty}^{\infty} x[n] e^{-j\Omega n}$ to our previous equation:

Since $x[n] = 0$ for $n < 0$ (due to the unit step function $u[n]$), we can rewrite the summation for $n \geq 0$ as follows:

$$X(e^{i\Omega}) = \sum_{n=0}^{\infty}\left(\sum_{k=1}^{K} G_k a_k^n\right)\cdot e^{-i\Omega n} \tag{A2}$$

Observe that we have disregarded for now the rubbery modulus $\{G_e\}$ term for tidiness in the derivation, but its DTFT will be added in the end thanks to the linearity of the DTFT, which allows us to treat it separately. Now, let us exchange the order of the summations:

$$X(e^{i\Omega}) = \sum_{k=1}^{K}\left(G_k\sum_{n=0}^{\infty}(a_k^n\cdot e^{-i\Omega n})\right) \tag{A3}$$

We can rewrite the inner summation as a geometric series (Kreyszig, 1999):

$$X(e^{i\Omega}) = \sum_{k=1}^{K} G_k\sum_{n=0}^{\infty}(a_k e^{-i\Omega})^n \tag{A4}$$

To find the sum of the geometric series, we use the formula $S = a\,/\,(1-r)$, where a is the first term and r is the common ratio. In this case, $a = 1$ (when $n = 0$) and $r = a_k e^{-\mathrm{i}\Omega}$. So, the sum of the geometric series is:

$$S_k = \frac{1}{1-a_k e^{-i\Omega}}$$

Now, we sum over all values of k (from $k = 1$ to $k = K$):

$$X(e^{i\Omega}) = \sum_{k=1}^{K} G_k\frac{1}{1-a_k e^{-i\Omega}} \tag{A5}$$

We then add the contribution from the rubbery modulus term $\{G_e\}$ which is a constant multiplied by the unit step function in Equation (A1). The DTFT of the unit step function is $U(e^{i\Omega}) = \frac{1}{1-e^{-i\Omega}} + \sum_{r=-\infty}^{\infty}\pi\delta(\Omega-2\pi\mathrm{r})$

(Oppenheim et al., 1999). Thus, the DTFT of $\{G_e\}\cdot u[n]$ is $\frac{\{G_e\}}{1-e^{-i\Omega}} + \{G_e\}\sum_{r=-\infty}^{\infty}\pi\delta(\Omega-2\pi\mathrm{r})$ and can be added to Equation (A5). Finally, substituting $a_k = e^{-\Delta t/\tau_k}, \quad k = 1,2,\ldots,K$ we obtain our final expression for Equation (11) in the main manuscript:

$$X(e^{i\Omega}) = \Delta t\frac{\{G_e\}}{1-e^{-i\Omega}} + \Delta t\{G_e\}\sum_{r=-\infty}^{\infty}\pi\delta(\Omega-2\pi\mathrm{r}) + \Delta t\sum_{k=1}^{K}\frac{G_k}{1-e^{-\Delta t/\tau_k}e^{-i\Omega}} \tag{A6}$$

Where Δt is added for normalization of the DTFT since the horizontal spacing of the time sequence is Δt in the Riemann sum defined by the DTFT.

At this point we proceed to compare the DTFT latest equation with the CTFT, in order to study the effect of aliasing. It is illustrative to perform a Taylor series expansion on the exponential terms in the denominator, so both equations are closer in appearance.

By performing a Taylor series expansion of the exponential term containing the characteristic times, we obtain:

$$e^{-\frac{\Delta t}{\tau_k}} = 1-\frac{\Delta t}{\tau_k}+\frac{(\Delta t/\tau_k)^2}{2!}-\frac{(\Delta t/\tau_k)^3}{3!}+\cdots$$

For small $\frac{\Delta t}{\tau_k}$ (to mitigate aliasing), we can keep up to the 2nd term in the series. Then, similarly:

$$e^{-i\omega\Delta t} = 1-i\omega\Delta t-\frac{(\omega\Delta t)^2}{2!}+i\frac{(\omega\Delta t)^3}{3!}+\frac{(\omega\Delta t)^4}{4!}-i\frac{(\omega\Delta t)^5}{5!}-\cdots$$

Keeping up to the 2nd term again, Equation (A6) becomes:

$$X(e^{i\omega\Delta t}) \approx \Delta t\frac{\{G_e\}}{1-(1-i\omega\Delta t)} + \sum_{k=1}^{K}\frac{\Delta t G_k}{1-(1-\Delta t/\tau_k)(1-i\omega\Delta t)} \tag{A7}$$

Expanding the denominator:

$$X(e^{i\omega\Delta t}) \approx \Delta t \frac{\{G_e\}}{1-1+i\omega\Delta t} + \Delta t\{G_e\} \sum_{r=-\infty}^{\infty} \pi\delta(\Omega - 2\pi\mathrm{r}) + \sum_{k=1}^{K} \frac{\Delta t G_k}{(i\omega\Delta t + \Delta t/\tau_k - i\omega\Delta t^2/\tau_k)}$$

Simplifying we arrive at Equation (12) in the main manuscript that is similar in form to the theoretical time-continuous case (Equation (3)). This is the expression we use in the main manuscript for our discussion of frequency aliasing as it explicitly shows it in the $i\omega\Delta t$ term in the denominator, which is the "extra" term with respect to the theoretical continuous-time case (Equation (3)):

$$X(e^{i\omega\Delta t}) \sim \{G_e\}\left(\frac{1}{i\omega} + \Delta t \sum_{r=-\infty}^{\infty} \pi\delta(\Omega - 2\pi r)\right) + \sum_{k=1}^{K} \frac{G_k\tau_k}{1 + i\omega\tau_k - i\omega\Delta t} \tag{A8}$$

Appendix 2: Derivation of DTFT for a finite M-size sequence

Now we turn our attention to the case of the finite M-element sequence, where we also ignore for now G_e rubbery modulus:

$$y[n] = (u[n] - u[M]) \cdot \left(\sum_{k=1}^{K} G_k a_k^n + \{G_e\}\right), \quad n = 1,2,\ldots,\infty \tag{A9}$$

where $a_k = e^{-\Delta t/\tau_k}, \quad k = 1,2,\ldots,K.$

The DTFT is defined as a Riemann sum: $Y(e^{i\Omega}) = \sum_{n=-\infty}^{\infty} y[n]\, e^{-i\Omega n}$ and is applied to our previous equation. For the time being, we drop the $\{G_e\}$ constant term whose contribution will be added at the end (by linearity of DTFT), for tidiness in the derivation.

For $n < 0$ the terms are zero so we can rewrite the summation for $n \geq 1$:

$$Y(e^{i\Omega}) = \sum_{n=1}^{\infty} \left((u[n] - u[n-M]) \left(\sum_{k=1}^{K} G_k a_k^n \right) \right) e^{-i\Omega n} \tag{A10}$$

We can split the summation into two parts, one with $u[n]$ and the other with $u[n - M]$:

$$Y(e^{i\Omega}) = \sum_{n=1}^{\infty} u[n] \left(\sum_{k=1}^{K} G_k a_k^n \right) e^{-i\Omega n} - \sum_{n=1}^{\infty} u[n-M] \left(\sum_{k=1}^{K} G_k a_k^n \right) e^{-i\Omega n} \tag{A11}$$

Let us compute the DTFT of each part separately: $Y(e^{i\Omega}) = X_1(e^{i\Omega}) - X_2(e^{i\Omega})$

For the first part:

$$X_1(e^{i\Omega}) = \sum_{n=1}^{\infty} u[n] \left(\sum_{k=1}^{K} G_k a_k^n \right) e^{-i\Omega n} \tag{A12}$$

Since $u[n] = 0$ for $n < 0$, we can rewrite the summation for $n \geq 0$:

$$X_1(e^{i\Omega}) = \sum_{n=0}^{\infty} \left(\sum_{k=1}^{K} G_k a_k^n \right) e^{-i\Omega n} \tag{A13}$$

Following the same steps as in Appendix 1:

$$X_1(e^{i\Omega}) = \sum_{k=1}^{K} G_k \frac{1}{1 - a_k e^{-i\Omega}} \tag{A14}$$

For the second part:

$$X_2(e^{i\Omega}) = \sum_{n=1}^{\infty} u[n-M]\left(\sum_{k=1}^{K} G_k a_k^n\right) e^{-i\Omega n} \tag{A15}$$

Since $u[n\ -\ M]\ =\ 0$ for $n\ <\ M$, we can rewrite the summation for $n\ \geq\ M$:

$$X_2(e^{i\Omega}) = \sum_{n=M}^{\infty}\left(\sum_{k=1}^{K} G_k a_k^n\right) e^{-i\Omega n} \tag{A16}$$

We can rewrite the summation with a change of variable $p\ =\ n\ -\ M$:

$$X_2(e^{i\Omega}) = \sum_{p=0}^{\infty}\left(\sum_{k=1}^{K} G_k a_k^{p+M}\right) e^{-i\Omega(p+M)} \tag{A17}$$

Factoring out $e^{-i\Omega M}$

$$X_2(e^{i\Omega}) = e^{-i\Omega M}\sum_{p=0}^{\infty}\left(\sum_{k=1}^{K} G_k a_k^M\left(a_k^p\right)\right) e^{-i\Omega p} \tag{A18}$$

Now, the inner summation is a geometric series just like in the previous Appendix:

$$X_2(e^{i\Omega}) = e^{-i\Omega M} * \sum_{k=1}^{K} G_k a_k^M \frac{1}{1-a_k e^{-i\Omega}} \tag{A19}$$

Now, let us combine both parts to find the DTFT of the sequence $y[n]$:

$$Y(e^{i\Omega}) = X_1(e^{i\Omega}) - X_2(e^{i\Omega})$$

$$Y(e^{i\Omega}) = \sum_{k=1}^{K} G_k \frac{1}{1-a_k e^{-i\Omega}} - e^{-i\Omega M}\sum_{k=1}^{K} G_k a_k^M \frac{1}{1-a_k e^{-i\Omega}} \tag{A20}$$

Substituting back $a_k = e^{-\Delta t/\tau_k}$ and multiplying by Δt for the Riemann sum normalization, we obtain:

$$Y(e^{i\Omega}) = \Delta t \sum_{k=1}^{K} \frac{G_k(1-e^{-M\Delta t/\tau_k} e^{-j\Omega M})}{1-e^{-\Delta t/\tau_k} e^{-j\Omega}} \tag{A21}$$

For completeness let's include the rubbery modulus term as it is relevant in certain cases. In other words, we now turn attention to Equation (A9) with the added G_e term as it may be part of the time-relaxation function:

$$y[n] = (u[n]-u[M])\cdot\left(\sum_{k=1}^{K} G_k a_k^n + G_e\right), \quad n = 1,2,\ldots,\infty \tag{A22}$$

By the linearity of the DTFT, we can address this by separate parts, and then add them up:

$$y[n] = (u[n]-u[M])\cdot\left(\sum_{k=1}^{K} G_k a_k^n\right) + (u[n]-u[M])\cdot G_e, \quad n = 1,2,\ldots,\infty$$

The DTFT of the first term is Equation (A21). now we are interested in the DTFT of $(u[n]-u[M])\cdot G_e$,

$$Y_2(e^{i\omega}) = \sum_{n=-\infty}^{\infty}(G_e(u[n]-u[n-M])\cdot e^{-i\Omega n}) \tag{A23}$$

Since $u[n]\ =\ 1$ for $n\ >=\ 0$ and $u[n]\ =\ 0$ for $n\ <\ 0$, and $u[n\ -\ M]\ =\ 1$ for $n\ >=\ M$ and $u[n\ -\ M]\ =\ 0$ for $n\ <\ M$, the sum becomes:

$$Y_2(e^{i\omega}) = G_e\sum_{n=0}^{M-1}\left((1-0)\cdot e^{-i\Omega n}\right)$$

$$Y_2(e^{i\omega}) = G_e\sum_{n=0}^{M-1}(e^{-i\Omega n})$$

Now, we can compute the sum using the formula for the finite geometric series:

$$Y_2(e^{i\omega}) = G_e \frac{1 - e^{-i\Omega M}}{1 - e^{-i\Omega}}$$

Now we can add this expression to Equation (A21) to get the DTFT of Equation (A22), which coincides with Equation (15) in the main manuscript:

$$Y(e^{i\Omega}) = \Delta t \sum_{k=1}^{K} \frac{G_k(1 - e^{-M\Delta t/\tau_k} e^{-i\Omega M})}{1 - e^{-\Delta t/\tau_k} e^{-i\Omega}} + \Delta t \left\{ \frac{G_e(1 - e^{-i\Omega M})}{1 - e^{-i\Omega}} \right\} \tag{A24}$$

Here again we perform Taylor series expansion substitutions. First, we perform a Taylor series expansion of the exponential term containing the characteristic times:

$$e^{-\frac{\Delta t}{\tau_k}} = 1 - \frac{\Delta t}{\tau_k} + \frac{(\Delta t/\tau_k)^2}{2!} - \frac{(\Delta t/\tau_k)^3}{3!} + \cdots$$

For small $\frac{\Delta t}{\tau_k}$ (to mitigate aliasing), we can approximate it up to the 2nd term. Then similarly:

$$e^{-i\omega\Delta t} = 1 - i\omega\Delta t - \frac{(\omega\Delta t)^2}{2!} + i\frac{(\omega\Delta t)^3}{3!} + \frac{(\omega\Delta t)^4}{4!} - i\frac{(\omega\Delta t)^5}{5!} - \cdots$$

Now we substitute the Taylor series up to the second term:

$$Y(e^{i\omega\Delta t}) \approx \Delta t \sum_{k=1}^{K} \frac{G_k}{1 - (1 - \Delta t/\tau_k)(1 - i\omega\Delta t)} - \Delta t \sum_{k=1}^{K} \frac{G_k e^{-M\Delta t/\tau_k} e^{-i\omega\Delta t M}}{1 - (1 - \Delta t/\tau_k)(1 - i\omega\Delta t)} + \Delta t \left\{ \frac{G_e(1 - e^{-i\omega\Delta t M})}{1 - (1 - i\omega\Delta t)} \right\} \tag{A25}$$

Expanding the denominators:

$$Y(e^{i\omega\Delta t}) \approx \Delta t \sum_{k=1}^{K} \frac{G_k}{(i\omega\Delta t + \Delta t/\tau_k - i\omega\Delta t^2/\tau_k)} - \Delta t \sum_{k=1}^{K} \frac{G_k e^{-M\Delta t/\tau_k} e^{-j\omega\Delta t M}}{(i\omega\Delta t + \Delta t/\tau_k - i\omega\Delta t^2/\tau_k)} + \Delta t \left\{ \frac{G_e(1 - e^{-i\omega\Delta t M})}{1 - 1 + i\omega\Delta t)} \right\} \tag{A26}$$

Simplifying:

$$Y(e^{i\omega\Delta t}) \approx \sum_{k=1}^{K} \frac{G_k\tau_k}{(i\omega\tau_k + 1 - i\omega\Delta t)} - \sum_{k=1}^{K} \frac{\tau_k G_k e^{-M\Delta t/\tau_k} e^{-j\omega\Delta t M}}{(i\omega\tau_k + 1 - i\omega\Delta t)} + \Delta t \left\{ \frac{G_e(1 - e^{-i\omega\Delta t M})}{i\omega\Delta t} \right\} \tag{A27}$$

Factoring out we arrive at our final expression in the main manuscript for the DTFT of a discrete and finite stress relaxation sequence (Equation (16)):

$$Y(e^{i\omega\Delta t}) \approx \Delta t \sum_{k=1}^{K} \frac{G_k\tau_k(1 - e^{-M\Delta t/\tau_k} e^{-i\omega\Delta t M})}{(i\omega\tau_k + 1 - i\omega\Delta t)} + \left\{ \frac{G_e(1 - e^{-i\omega\Delta t M})}{i\omega} \right\} \tag{A28}$$

The Riemann sum normalization factor Δt is included here as well.